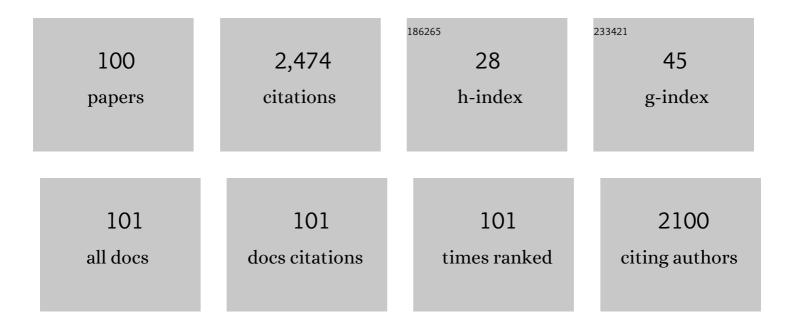
Jun-Sang Park

List of Publications by Year in descending order

Source: https://exaly.com/author-pdf/4031751/publications.pdf Version: 2024-02-01



ILIN-SANC DADK

#	Article	IF	CITATIONS
1	Direct measurement of critical resolved shear stress of prismatic and basal slip in polycrystalline Ti using high energy X-ray diffraction microscopy. Acta Materialia, 2017, 132, 598-610.	7.9	146
2	On the measurement of dislocations and dislocation substructures using EBSD and HRSD techniques. Acta Materialia, 2019, 175, 297-313.	7.9	128
3	Modeling slip system strength evolution in Ti-7Al informed by in-situ grain stress measurements. Acta Materialia, 2017, 128, 406-417.	7.9	97
4	Investigation of fatigue crack initiation from a non-metallic inclusion via high energy x-ray diffraction microscopy. Acta Materialia, 2017, 137, 71-84.	7.9	92
5	Study of slip activity in a Mg-Y alloy by in situ high energy X-ray diffraction microscopy and elastic viscoplastic self-consistent modeling. Acta Materialia, 2018, 155, 138-152.	7.9	90
6	Effect of heat treatment on the tensile behavior of selective laser melted Ti-6Al-4V by in situ X-ray characterization. Acta Materialia, 2020, 189, 93-104.	7.9	88
7	Highly deformable Mg–Al–Ca alloy with Al2Ca precipitates. Acta Materialia, 2020, 200, 236-245.	7.9	81
8	Synchrotron Imaging of Pore Formation in Li Metal Solid-State Batteries Aided by Machine Learning. ACS Applied Energy Materials, 2020, 3, 9534-9542.	5.1	75
9	Role of heat treatment and build orientation in the microstructure sensitive deformation characteristics of IN718 produced via SLM additive manufacturing. Additive Manufacturing, 2018, 22, 479-496.	3.0	58
10	Experimental measurement of lattice strain pole figures using synchrotron x rays. Review of Scientific Instruments, 2005, 76, 113903.	1.3	54
11	Study of grain-level deformation and residual stresses in Ti-7Al under combined bending and tension using high energy diffraction microscopy (HEDM). International Journal of Solids and Structures, 2016, 94-95, 35-49.	2.7	54
12	Measuring and modeling distributions of stress state in deforming polycrystals. Acta Materialia, 2008, 56, 3927-3939.	7.9	53
13	Measuring Stress Distributions in Ti-6Al-4V Using Synchrotron X-Ray Diffraction. Metallurgical and Materials Transactions A: Physical Metallurgy and Materials Science, 2008, 39, 3120-3133.	2.2	50
14	On the microstructure and strengthening mechanism in oxide dispersion-strengthened 316 steel: A coordinated electron microscopy, atom probe tomography and in situ synchrotron tensile investigation. Materials Science & amp; Engineering A: Structural Materials: Properties, Microstructure and Processing, 2015, 639, 585-596.	5.6	48
15	Effect of water on nanomechanics of bone is different between tension and compression. Journal of the Mechanical Behavior of Biomedical Materials, 2016, 57, 128-138.	3.1	44
16	Status and prospect of <i>in situ</i> and <i>operando</i> characterization of solid-state batteries. Energy and Environmental Science, 2021, 14, 4672-4711.	30.8	44
17	Determining the strengths of HCP slip systems using harmonic analyses of lattice strain distributions. Acta Materialia, 2018, 144, 92-106.	7.9	42
18	In situ high-energy X-ray diffraction study of tensile deformation of neutron-irradiated polycrystalline Fe-9%Cr alloy. Acta Materialia, 2017, 126, 67-76.	7.9	41

#	Article	IF	CITATIONS
19	A framework for generating synthetic diffraction images from deforming polycrystals using crystal-based finite element formulations. Computational Materials Science, 2013, 77, 456-466.	3.0	40
20	Origins of high ductility exhibited by an extruded magnesium alloy Mg-1.8Zn-0.2Ca: Experiments and crystal plasticity modeling. Journal of Materials Science and Technology, 2021, 84, 27-42.	10.7	39
21	Mechanical twinning and detwinning in pure Ti during loading and unloading – An in situ high-energy X-ray diffraction microscopy study. Scripta Materialia, 2014, 92, 35-38.	5.2	38
22	Influences of granular constraints and surface effects on the heterogeneity of elastic, superelastic, and plastic responses of polycrystalline shape memory alloys. Journal of the Mechanics and Physics of Solids, 2017, 102, 46-66.	4.8	38
23	A methodology to determine the elastic moduli of crystals by matching experimental and simulated lattice strain pole figures using discrete harmonics. Acta Materialia, 2017, 126, 469-480.	7.9	37
24	A method for measuring single-crystal elastic moduli using high-energy X-ray diffraction and a crystal-based finite element model. Acta Materialia, 2010, 58, 5806-5819.	7.9	34
25	Eliminating the non-Gaussian spectral response of X-ray absorbers for transition-edge sensors. Applied Physics Letters, 2017, 111, .	3.3	33
26	In situ high energy X-ray diffraction measurement of strain and dislocation density ahead of crack tips grown in hydrogen. Acta Materialia, 2019, 180, 272-286.	7.9	33
27	Direct observations and characterization of crack closure during microstructurally small fatigue crack growth via in-situ high-energy X-ray characterization. Acta Materialia, 2021, 205, 116564.	7.9	33
28	The comparison of microstructures and mechanical properties between 14Cr-Al and 14Cr-Ti ferritic ODS alloys. Materials and Design, 2016, 98, 61-67.	7.0	29
29	Effects of heat treatment and build orientation on the evolution of ϵ and α′ martensite and strength during compressive loading of additively manufactured 304L stainless steel. Acta Materialia, 2020, 195, 59-70.	7.9	29
30	In situ high-energy X-ray diffraction mapping of Lüders band propagation in medium-Mn transformation-induced plasticity steels. Materials Research Letters, 2018, 6, 662-667.	8.7	28
31	A complete grain-level assessment of the stress-strain evolution and associated deformation response in polycrystalline alloys. Acta Materialia, 2020, 201, 36-54.	7.9	27
32	Fiducial marker application method for position alignment of <i>in situ</i> multimodal X-ray experiments and reconstructions. Journal of Applied Crystallography, 2016, 49, 700-704.	4.5	26
33	Modeling Ti–6Al–4V using crystal plasticity, calibrated with multi-scale experiments, to understand the effect of the orientation and morphology of the α and β phases on time dependent cyclic loading. Journal of the Mechanics and Physics of Solids, 2021, 146, 104192.	4.8	26
34	In situ synchrotron X-ray diffraction study of hydrides in Zircaloy-4 during thermomechanical cycling. Journal of Nuclear Materials, 2017, 487, 247-259.	2.7	24
35	Sparse recovery of undersampled intensity patterns for coherent diffraction imaging at high X-ray energies. Scientific Reports, 2018, 8, 4959.	3.3	24
36	Quantifying Three-Dimensional Residual Stress Distributions Using Spatially-Resolved Diffraction Measurements and Finite Element Based Data Reduction. Experimental Mechanics, 2013, 53, 1491-1507.	2.0	23

#	Article	IF	CITATIONS
37	Analyzing shear band formation with high resolution X-ray diffraction. Acta Materialia, 2018, 147, 133-148.	7.9	22
38	Bright x-rays reveal shifting deformation states and effects of the microstructure on the plastic deformation of crystalline materials. Physical Review B, 2017, 96, .	3.2	21
39	Strain rate sensitivity, microstructure variations, and stress-assisted βÂ→Âα′′ phase transformation investigation on the mechanical behavior of dual-phase titanium alloys. Materials Characterization, 2020, 166, 110410.	4.4	20
40	High-energy synchrotron x-ray techniques for studying irradiated materials. Journal of Materials Research, 2015, 30, 1380-1391.	2.6	19
41	In situ synchrotron tensile investigations on 14YWT, MA957, and 9-Cr ODS alloys. Journal of Nuclear Materials, 2016, 471, 289-298.	2.7	19
42	Intermittent plasticity in individual grains: A study using high energy x-ray diffraction. Structural Dynamics, 2019, 6, 014501.	2.3	19
43	<i>BraggNN</i> : fast X-ray Bragg peak analysis using deep learning. IUCrJ, 2022, 9, 104-113.	2.2	19
44	A computational framework for evaluating residual stress distributions from diffraction-based lattice strain data. Computer Methods in Applied Mechanics and Engineering, 2013, 265, 120-135.	6.6	18
45	High-energy synchrotron study of in-pile-irradiated U–Mo fuels. Scripta Materialia, 2016, 114, 146-150.	5.2	18
46	Correlation of precipitate evolution with Vickers hardness in Haynes® 282® superalloy: In-situ high-energy SAXS/WAXS investigation. Materials Science & Engineering A: Structural Materials: Properties, Microstructure and Processing, 2018, 711, 250-258.	5.6	18
47	High-energy synchrotron x-ray study of deformation-induced martensitic transformation in a neutron-irradiated Type 316 stainless steel. Acta Materialia, 2020, 200, 315-327.	7.9	18
48	Microstructure Development of 308L Stainless Steel During Additive Manufacturing. Metallurgical and Materials Transactions A: Physical Metallurgy and Materials Science, 2019, 50, 2538-2553.	2.2	17
49	ICME Approach to Determining Critical Pore Size of IN718 Produced by Selective Laser Melting. Jom, 2020, 72, 465-474.	1.9	17
50	In situ synchrotron investigation of grain growth behavior of nano-grained UO2. Scripta Materialia, 2017, 131, 29-32.	5.2	16
51	In-situ high-energy X-ray characterization of neutron irradiated HT-UPS stainless steel under tensile deformation. Acta Materialia, 2018, 156, 330-341.	7.9	16
52	Phase retrieval for Bragg coherent diffraction imaging at high x-ray energies. Physical Review A, 2019, 99, .	2.5	15
53	Load-partitioning in an oxide dispersion-strengthened 310 steel at elevated temperatures. Materials and Design, 2016, 111, 622-630.	7.0	14
54	iRadMat: A thermo-mechanical testing system for in situ high-energy X-ray characterization of radioactive specimens. Review of Scientific Instruments, 2017, 88, 015111.	1.3	14

#	Article	IF	CITATIONS
55	Elucidating the temperature dependence of TRIP in Q&P steels using synchrotron X-Ray diffraction, constituent phase properties, and strain-based kinetics models. Acta Materialia, 2022, 237, 118126.	7.9	14
56	A methodology for measuring in situ lattice strain of bulk polycrystalline material under cyclic load. Review of Scientific Instruments, 2007, 78, 023910.	1.3	13
57	Quantitative Stress Analysis of Recrystallized OFHC Cu Subject to Deformation In Situ. Journal of Engineering Materials and Technology, Transactions of the ASME, 2008, 130, .	1.4	13
58	Void coalescence and ductile failure in IN718 investigated via high-energy synchrotron X-ray tomography and diffraction. Journal of the Mechanics and Physics of Solids, 2020, 145, 104155.	4.8	13
59	Transformative high entropy alloy conquers the strength-ductility paradigm by massive interface strengthening. Scripta Materialia, 2021, 203, 114070.	5.2	13
60	Determination of residual stress in a microtextured <i>α</i> titanium component using high-energy synchrotron X-rays. Journal of Strain Analysis for Engineering Design, 2016, 51, 358-374.	1.8	12
61	Non-Destructive Characterization of Engineering Materials Using High-Energy X-rays at the Advanced Photon Source. Synchrotron Radiation News, 2017, 30, 9-16.	0.8	12
62	AFRL Additive Manufacturing Modeling Series: Challenge 4, In Situ Mechanical Test of an IN625 Sample with Concurrent High-Energy Diffraction Microscopy Characterization. Integrating Materials and Manufacturing Innovation, 2021, 10, 338-347.	2.6	12
63	Synchrotron x-ray diffraction and crystal plasticity modeling study of martensitic transformation, texture development, and stress partitioning in deep-drawn TRIP steels. Materialia, 2021, 18, 101162.	2.7	11
64	Deep learning approaches to semantic segmentation of fatigue cracking within cyclically loaded nickel superalloy. Computational Materials Science, 2021, 198, 110683.	3.0	11
65	Characterization of neutron-irradiated HT-UPS steel by high-energy X-ray diffraction microscopy. Journal of Nuclear Materials, 2016, 471, 280-288.	2.7	10
66	Validating a Model for Welding Induced Residual Stress Using High-Energy X-ray Diffraction. Jom, 2017, 69, 893-899.	1.9	10
67	Far-Field High-Energy Diffraction Microscopy: A Non-Destructive Tool for Characterizing the Microstructure and Micromechanical State of Polycrystalline Materials. Microscopy Today, 2017, 25, 36-45.	0.3	10
68	In situ high-energy X-ray study of deformation mechanisms in additively manufactured 316L stainless steel. Journal of Nuclear Materials, 2021, 549, 152874.	2.7	10
69	Investigation of High-Energy Ion-Irradiated MA957 Using Synchrotron Radiation under In-Situ Tension. Materials, 2016, 9, 15.	2.9	9
70	A Planar Biaxial Experiment Platform for In Situ High-Energy Diffraction Studies. Experimental Mechanics, 2019, 59, 749-774.	2.0	9
71	Microstructure-Based Estimation of Strength and Ductility Distributions for \$\$alpha +eta \$\$ Titanium Alloys. Metallurgical and Materials Transactions A: Physical Metallurgy and Materials Science, 2021, 52, 2411-2434.	2.2	9
72	Thermal and Electric Field-Dependent Evolution of Domain Structures in Polycrystalline BaTiO3 Using the 3D-XRD Technique. Texture Stress and Microstructure, 2010, 2010, 1-10.	0.3	7

#	Article	IF	CITATIONS
73	Temperature effect of elastic anisotropy and internal strain development in advanced nanostructured alloys: An in-situ synchrotron X-ray investigation. Materials Science & Engineering A: Structural Materials: Properties, Microstructure and Processing, 2017, 692, 53-61.	5.6	7
74	High-energy x-ray diffraction microscopy study of deformation microstructures in neutron-irradiated polycrystalline Fe-9%Cr. Journal of Nuclear Materials, 2018, 508, 556-566.	2.7	7
75	Precipitate Characterization in Model Al-Zn-Mg-(Cu) Alloys Using Small-Angle X-ray Scattering. Metals, 2020, 10, 959.	2.3	7
76	In situ characterization of residual stress evolution during heat treatment of SiC/SiC ceramic matrix composites using highâ€energy Xâ€ray diffraction. Journal of the American Ceramic Society, 2021, 104, 1424-1435.	3.8	7
77	Precision lattice parameter determination from transmission diffraction of thick specimens with irregular cross sections. Journal of Applied Crystallography, 2019, 52, 40-46.	4.5	7
78	High-energy X-ray phase analysis of CMAS-infiltrated 7YSZ thermal barrier coatings: Effect of time and temperature. Journal of Materials Research, 2020, 35, 2300-2310.	2.6	6
79	Tensile behavior and microstructural evolution of a Fe-25Ni-20Cr austenitic stainless steel (alloy 709) from room to elevated temperatures through in-situ synchrotron X-ray diffraction characterization and transmission electron microscopy. Journal of Nuclear Materials, 2020, 540, 152367.	2.7	6
80	Evaluating the Taylor hardening model in polycrystalline Ti using high energy X-ray diffraction microscopy. Scripta Materialia, 2021, 195, 113743.	5.2	6
81	Repeatability and sensitivity characterization of the far-field high-energy diffraction microscopy instrument at the Advanced Photon Source. Journal of Synchrotron Radiation, 2021, 28, 1786-1800.	2.4	6
82	Residual Strain Analysis in Linear Friction Welds of Similar and Dissimilar Titanium Alloys Using Energy Dispersive X-ray Diffraction. Metallurgical and Materials Transactions A: Physical Metallurgy and Materials Science, 2019, 50, 704-718.	2.2	5
83	Data management and processing workflow for the Materials Physics and Engineering group beamlines at the Advanced Photon Source. Journal of Synchrotron Radiation, 2019, 26, 373-381.	2.4	5
84	A study on texture stability and the biaxial creep behavior of as-hydrided CWSR Zircaloy-4 cladding at the effective stresses from 55ÂMPa to 65ÂMPa and temperatures from 300°C to 400°C. Journal of Nuclear Materials, 2022, 564, 153688.	2.7	5
85	Microstructure Analysis of Bismuth Absorbers for Transition-Edge Sensor X-ray Microcalorimeters. Journal of Low Temperature Physics, 2018, 193, 225-230.	1.4	4
86	Measurement of Residual Stresses in Different Thicknesses of Laser Shock Peened Aluminium Alloy Samples. , 2018, , .		4
87	In situ synchrotron tensile investigations on ultrasonic additive manufactured (UAM) zirconium. Journal of Nuclear Materials, 2022, 568, 153843.	2.7	4
88	Demonstration of a chamber for strain mapping of steel specimens under mechanical load in a hydrogen environment by synchrotron radiation. Review of Scientific Instruments, 2018, 89, 063701.	1.3	3
89	Non-Destructive Internal Lattice Strain Measurement Using High Energy Synchrotron Radiation. Conference Proceedings of the Society for Experimental Mechanics, 2017, , 121-126.	0.5	3
90	Developing ductile and isotropic Ti alloy with tailored composition for laser powder bed fusion. Additive Manufacturing, 2022, 52, 102656.	3.0	3

#	Article	IF	CITATIONS
91	Non-Destructive Characterization of Subsurface Residual Stress Fields and Correlation with Microstructural Conditions in a Shot-Peened Inconel Component. Experimental Mechanics, 2018, 58, 1389-1406.	2.0	2
92	Comparison of Electron-Beam Physical Vapor Deposition and Plasma-Spray Physical Vapor Deposition Thermal Barrier Coating Properties Using Synchrotron X-Ray Diffraction. , 2019, , .		2
93	AFRL Additive Manufacturing Modeling Series: Challenge 1, Characterization of Residual Strain Distribution in Additively-Manufactured Metal Parts Using Energy-Dispersive Diffraction. Integrating Materials and Manufacturing Innovation, 2021, 10, 525.	2.6	2
94	Time-resolved phase and compositional homogenization of segregated uranium-niobium alloys above the monotectoid temperature. Journal of Nuclear Materials, 2022, 564, 153673.	2.7	2
95	Revealing the chemical environment of Cr, Fe, and Ni in high temperature-ultrafine precipitate strengthened steel subjected to low fluence neutron irradiation. Journal of Nuclear Materials, 2021, 554, 153056.	2.7	1
96	Microstructure and Deformation Behavior of Thermally Aged Cast Austenitic Stainless Steels. Minerals, Metals and Materials Series, 2018, , 625-641.	0.4	1
97	A New Residual Strain Mapping Program Using Energy Dispersive X-Ray Diffraction at the Advanced Photon Source. Experimental Mechanics, 2022, 62, 1363-1379.	2.0	1
98	Comparison of thermally cycled PS-PVD and EB-PVD thermal barrier coatings' depth-resolved monoclinic phase evolution via synchrotron X-ray diffraction. , 2020, , .		0
99	Synchrotron XRD Measurements of Thermal Barrier Coating Configurations With Rare Earth Elements for Phosphor Thermometry. , 2019, , .		0
100	4D evolution of Cr23C6 precipitates in neutron-irradiated and annealed HT-UPS steel observed via synchrotron micro-computed tomography. Journal of Materials Research, 2022, 37, 208-224.	2.6	0